Self-healing Chitosan-based Hydrogels as a Potential Platform for Enhanced Hemostasis

Tianji Li,[a,b] Chunli Wei,[c] Jinghua Yang,[c] Layun Deng,[d,*] Jianan Lan,[e] Jianwei Zhang,[f,*] Cheng Li,[f] and Shuai Xue,[a,c,e,*]

Injectable self-healing hydrogels are promising biomaterials for wound management, as their ability to autonomously repair enables conformal sealing of irregular wounds. In this study, an injectable hydrogel was fabricated through Schiff base cross-linking of acrylamide-modified chitosan (AMCS) and 50% oxidized alginate (ADA). To enhance its mechanical robustness and hemostatic performance, chitin nanogels (CNGs) were incorporated as a reinforcing component. The structure-property relationships of the resulting hydrogel were characterized using infrared spectroscopy, field emission scanning electron microscopy, confocal laser scanning microscopy, and rheological analysis. Rheological studies confirmed that the composite hydrogel (AANGH) exhibited a superior storage modulus and more robust self-healing recovery compared to the base hydrogel (AAH3). MTT assays using L929 fibroblast cells demonstrated outstanding cytocompatibility, with cell viability maintained at over 100%. Furthermore, *in vivo* hemostatic assessment demonstrated effective hepatic hemorrhage control, characterized by significantly reduced blood loss, shortened hemostasis time, and favorable antibacterial properties. This work establishes that AANGH is an effective strategy for creating a mechanically robust, self-healing, and highly biocompatible chitosan-based hydrogel with strong potential for hemostatic applications.

DOI: 10.15376/biores.21.1.2438-2453

Keywords: Self-healing; Chitosan; Hydrogel; Natural polymer; Hemostatic material; Biomedical

Contact information: a: Department of Hepatopancreatobiliary Surgery; Clinical Systems Biology Laboratories, Translational Medicine Center, The First Affiliated Hospital of Zhengzhou University, Zhengzhou 450001, China; b: School of Earth and Space Science and Technology, Wuhan University, Wuhan, China; c: Clinical Systems Biology Laboratories, Translational Medicine Center, The First Affiliated Hospital of Zhengzhou University, Zhengzhou 450001, China, 135065; d: State Key Laboratory of Woody Oil Resources Utilization, Hunan Academy of Forestry, Changsha 410018, China; e: Zhongnan Hospital of Wuhan University, Institute of Hepatobiliary Diseases of Wuhan University, Transplant Center of Wuhan University, Wuhan, China; f: College of Forestry, Henan Agricultural University, Zhengzhou 450002, China;
**Correspondence: deng269@163.com; zhangjianweiwhu@163.com; xueshuai_yfy@zzu.edu.cn*

INTRODUCTION

Effective hemostasis plays a vital role in trauma management and surgical interventions (Yang *et al.* 2023). Uncontrolled bleeding from critical organs or anatomically complex sites can rapidly lead to hemorrhagic shock, multi-organ dysfunction, and increased mortality (Qiao *et al.* 2021). Thus, timely and efficient hemostatic measures are essential for patient survival. Conventional methods, such as gauze packing, tourniquet application, and surgical suturing, are often inadequate in

achieving rapid hemostasis, limited by factors such as wound geometry, anatomical inaccessibility, and variations in vascular architecture (Ye *et al.* 2024). In recent years, a range of emerging hemostatic materials—including hemostatic clamps, bioadhesives, and advanced dressings—have been developed, yet their clinical application remains hampered by inherent shortcomings (Tompeck *et al.* 2020). For instance, hemostatic clamps demand considerable technical skill for effective use; particulate hemostatic powders often demonstrate inadequate tissue adhesion and carry risks of embolization due to migration under blood flow; and thrombogenic sponges frequently fail to conform effectively to irregular wound surfaces (Goncharuk *et al.* 2021). Therefore, there remains a pressing and unmet clinical need for innovative hemostatic strategies and engineered materials with improved performance and applicability.

Injectable hydrogels are pivotal in developing novel hemostatic agents. A key advantage is their geometry-adaptive nature, which allows them to fully conform to deep or irregular wound cavities, enabling effective non-compressive hemostasis through tissue adhesion while minimizing iatrogenic damage (Pourshahrestani *et al.* 2020). Their structural similarity to the extracellular matrix ensures excellent biocompatibility and controllable degradability, supporting use in biologically sensitive environments (Yang *et al.* 2024). The hydrophilic polymer networks maintain a moist wound interface, reducing friction and facilitating healing. To realize these advantages, the selection of appropriate and compatible biopolymers for constructing the hydrogel network is of fundamental criticality.

Chitosan (CS), the only naturally occurring alkaline polysaccharide composed of N-acetyl-d-glucosamine and β-(1–4)-linked d-glucosamine units, has garnered significant interest for addressing uncontrolled bleeding due to its favorable biocompatibility, biodegradability, and intrinsic bioactive properties (Bi *et al.* 2020). CS-based hydrogels, in particular, are valued for their tunable mechanical properties, injectability, and ability to promote hemostasis by absorbing red blood cells and activating platelets (Fan *et al.* 2023). However, a major practical limitation of chitosan lies in its solubility profile—it is only soluble in acidic aqueous media, which considerably restricts its processability and applicability under physiological conditions (Faizuloev *et al.* 2012). To overcome this challenge, carboxymethyl chitosan (CMCS) has been developed through chemical modification using monochloroacetic acid under alkaline conditions, which introduces carboxymethyl groups onto the polymer backbone (Cao *et al.* 2018). The resulting CMCS not only retains the inherent biocompatibility of chitosan but also exhibits markedly improved water solubility across a wider pH range (Vo *et al.* 2017). The coexistence of amino ($-NH_2$) and carboxyl ($-COOH$) groups within its structure imparts smart, stimuli-responsive functionality (Guo and Gao 2007), while its enhanced chemical reactivity, film- and gel-forming capabilities, and biodegradability collectively establish CMCS as a versatile and adaptive biomaterial (Zhang *et al.* 2024). This makes it highly promising for advanced hemostatic applications, where factors such as deacetylation degree, molecular weight, and chemical modification critically influence its performance in managing hemorrhage in skin, liver, arterial, and cardiac wounds (Zhang *et al.* 2024.)

Alginate is a naturally abundant polysaccharide composed of α-L-guluronate and β-D-mannuronate monomers, is widely recognized for its exceptional hydrophilicity, biocompatibility, and low toxicity, making it suitable for biomedical applications such as wound dressings and drug delivery (Zhao *et al.* 2023). However, its inherent hemostatic performance is primarily passive, relying on calcium-mediated gelation and fluid absorption, which remains limited for advanced, active therapeutic use. To address this,

chemical modification through periodate-mediated oxidation is employed. This reaction selectively cleaves the carbon-carbon bonds of the cis-diol groups on the sugar backbone, strategically converting hydroxyl groups into reactive aldehyde groups without disrupting the carboxylate functionalities (Liu *et al.* 2025). This transformation is pivotal, as the newly introduced aldehyde groups enable dynamic, covalent crosslinking *via* Schiff base chemistry. This allows the resulting oxidized alginate (ADA) to spontaneously conjugate with amine-containing polymers, such as chitosan, under physiological conditions without the need for harsh catalysts (Zhao *et al.* 2017), endowing alginate-derived materials with self-healing and injectable properties, significantly expanding their potential.

Therefore, CMCS and ADA are a rational polymer pair for constructing advanced hemostatic hydrogels. CMCS provides essential amine groups, inherent bioactivity, and adaptable functionality, while ADA offers complementary aldehyde groups for biocompatible crosslinking and enhanced hydrophilic matrix formation. Their combination through dynamic Schiff base chemistry allows for the fabrication of injectable, self-healing networks ideally suited for minimally invasive application to irregular wounds. To further augment the hemostatic efficacy of this system, it is proposed in this work to incorporate chitin nanogels (CNGs). It is hypothesized that CNG incorporation will significantly enhance hemostatic performance through a dual mechanism: (1) by providing nanoscale anchoring points to substantially improve wet tissue adhesive strength, ensuring robust sealing under dynamic bleeding conditions, and (2) by reinforcing the hydrogel matrix to better withstand blood pressure, optimize fluid absorption, and promote rapid clot stabilization (Ziaei *et al.* 2023).

Accordingly, the aims of this study were: (1) to synthesize and characterize the composite hydrogel (denoted as AANGH); (2) to evaluate its rheological, self-healing, and tissue-adhesive properties; and (3) to systematically assess its hemostatic performance and biocompatibility both in vitro and in vivo. The chemical structure and crosslinking were verified by Fourier transform infrared (FT-IR) spectroscopy. The internal microstructure and porosity were visualized using field emission scanning electron microscopy (FE-SEM) and confocal laser scanning microscopy (CLSM). Rheological analyses were conducted to evaluate the viscoelastic behavior. Furthermore, its potential biomedical applications were evaluated through cell and animal experiments in vitro and in vivo. All results confirmed the promising potential of this dynamic hydrogel system for biomedical applications, particularly in hemorrhage control and wound healing.

EXPERIMENTAL

Materials

Chitin, chitosan, urea, sodium hydroxide, sodium alginate, sodium periodate, acrylamide, and ethylene glycol were purchased from Shanghai Macklin Biochemical Co., Ltd., Zhengzhou Paini Chemical Reagent Factory, Shanghai Aladdin Biochemical Technology Co., Ltd., and Tianjin Fuyu Fine Chemical Co., Ltd., respectively. Concentrated hydrochloric acid, ethanol, and a 25% glutaraldehyde solution were obtained from Sinopharm Chemical Reagent Co., Ltd. Fetal bovine serum (FBS) and 3-(4,5-dimethylthiazol-2-yl)-2,5-diphenyltetrazolium bromide (MTT) were acquired from Gibco (USA). All chemical reagents were of analytical grade. Ultrapure water was used throughout the experiments.

Synthesis of 50% Oxidized Alginate (ADA50)

Oxidized alginate with a controlled oxidation degree of approximately 50% (ADA50) was synthesized to optimally balance the density of reactive aldehyde groups for efficient Schiff base cross-linking with chitosan derivatives and the preservation of the polymeric backbone integrity for maintaining adequate mechanical strength and controllable degradation of the resulting hydrogel. ADA50 was synthesized *via* periodate-mediated oxidation of sodium alginate, targeting a 50% theoretical oxidation degree of its diol units (Ravichandran *et al.* 2018). In a typical procedure, 20 g of sodium alginate was completely dissolved in 400 mL of ultrapure water under continuous mechanical stirring at ambient temperature. A sodium periodate solution (0.05 mol in 100 mL water) was then added dropwise to the mixture. The reaction was allowed to proceed for 6 h under light-protected conditions. To terminate the oxidation, 3.5 mL of 1,2-ethanediol was introduced, and stirring was continued for another 0.5 h at 25 °C to ensure complete quenching of residual periodate. The resulting mixture was then dialyzed extensively against deionized water to remove small-molecule byproducts and iodate salts. Finally, the purified product was lyophilized to obtain ADA50.

Synthesis of Acrylamide-Modified Chitosan (AMCS)

A 2 wt% chitosan precursor solution was first prepared by dissolving 4 g of chitosan in 196 g of an aqueous alkaline-urea solvent system (8 wt% NaOH, 4 wt% urea). The homogeneous mixture was stored at –20 °C for 36 h. During this period, it was subjected to two cycles of mechanical agitation and freeze–thawing to ensure molecular uniformity and improve homogeneity, yielding a clear, viscous solution. Subsequently, 6.173 g of acrylamide was added to 100 mL of this chitosan solution, achieving a 7:1 molar ratio of acrylamide to chitosan glucosamine units. The graft copolymerization was allowed to proceed under continuous stirring at 15 °C for 24 h. The resulting mixture was neutralized with dilute hydrochloric acid and centrifuged at 4000 rpm for 20 min to remove insoluble aggregates. The supernatant was collected, extensively dialyzed against deionized water for 7 days to eliminate unreacted monomers and salts, and finally lyophilized to obtain AMCS.

Preparation of Chitin Nanogel (CNGs)

Chitin nanogels (CNGs) were prepared using a cryo-dissolution and regeneration method. Briefly, 1.5 wt% chitin was dissolved in an aqueous alkaline solution containing 8 wt% NaOH and 4 wt% urea. The mixture was subjected to three consecutive freeze–thaw cycles at –25 °C to promote complete dissolution and form a transparent chitin solution. The solution was then subjected to high-shear homogenization at 10,000 rpm for 30 min to ensure a homogeneous dispersion of chitin nanofibrils. Following homogenization, the sample was centrifuged to remove residual impurities and undissolved aggregates. The resulting dispersion was extensively dialyzed against deionized water using a dialysis membrane (MWCO: 8 kDa) until the dialysate reached neutral pH, yielding a stable, aqueous dispersion of CNGs.

Synthesis of Chitin Nanogel-composite Self-healing Hydrogels

A series of self-healing hydrogels were fabricated through dynamic Schiff base crosslinking between AMCS and ADA50. Initially, 3 wt% AMCS stock solutions were prepared in either ultrapure water or a 0.5 wt% CNG dispersion. CNGs were incorporated into the network, aimed at improving mechanical strength, optimizing permeability and

fluid absorption to enhance overall hemostatic performance. The aqueous AMCS solution was then mixed with ADA50 at mass ratios (AMCS: ADA50) of 1:0.1, 1:0.3, and 1:0.6. The mixtures were gently stirred until ADA50 was fully dissolved and then allowed to stand for 10 min to form stable gels, which were designated as AAH1, AAH3, and AAH6, respectively. For the chitin nanogel-composite hydrogel, the AMCS/CNG stock solution was blended with ADA50 at a fixed mass ratio of 1:0.3. After gentle stirring and a 10-min gelation period, the resulting composite material was obtained and denoted as AANGH (approximately 4.4wt%).

Self-healing Property of the Hydrogel

As a proof of concept, a macroscopic cut-heal-stretch test was used to demonstrate the self-healing ability of the dynamic Schiff base network. Cylindrical specimens measuring 25.0 mm in diameter and 10.0 mm in height were prepared for this purpose. To enhance visual tracking of the healing process, rhodamine B dye was incorporated into the hydrogel matrix as a colorimetric indicator (Huang *et al.* 2021). In a typical experiment, each hydrogel cylinder was bisected into two halves using a sharp blade. The freshly cut surfaces were then gently brought into intimate contact and allowed to remain in place at ambient temperature (approximately 25 °C) without any external stimulus. After a healing period of 30 min, the autonomous self-repair capability was qualitatively assessed by carefully lifting the entire rejoined hydrogel from one end. The successful restoration of structural integrity was further confirmed by manually stretching the healed hydrogel to approximately twice its original length without fracture at the interface. This evaluation procedure was consistently applied to all hydrogel formulations, including AANGH, to ensure a comparative analysis under identical conditions.

FT-IR Spectroscopy

Fourier transform-infrared spectroscopy was employed to characterize the chemical structures and confirm the formation of dynamic covalent bonds in the hydrogel networks. Spectra of ADA50, AMCS, CNGs, AAH3, and AANGH were recorded on a Nicolet iS20 spectrometer (Thermo Fisher Scientific, USA) in absorbance mode using the conventional KBr pellet method. Prior to measurement, all solid samples were vacuum-dried and homogenized with spectroscopic-grade KBr. Each spectrum was acquired over the wavenumber range of 400 to 4000 cm^{-1} at a resolution of 4 cm^{-1}, accumulating 32 scans to ensure an adequate signal-to-noise ratio (Li *et al.* 2024). Background correction was performed using a pure KBr pellet under identical conditions. The resulting spectra were analyzed to identify characteristic absorption bands, providing definitive evidence of the chemical transformations during hydrogel formation.

Rheological Studies

To directly verify the rapid and reversible recovery of the hydrogel network's mechanical properties after severe shear disruption, rheological characterization of the self-healing hydrogels and AANGH was performed using a Discovery Hybrid Rheometer (DHR, TA Instruments, USA) equipped with a 40 mm diameter cone-plate geometry. All measurements were conducted at a constant temperature of 25 °C with a fixed gap distance of 1 mm. To evaluate the shear-induced recovery behavior of the hydrogels, oscillatory step-strain tests were conducted by cyclically alternating the strain amplitude between a low strain of 1% (within the linear viscoelastic region) and a high strain of 200% (inducing structural breakdown) at a constant angular frequency of 1.0 Hz. This sequence was

repeated for three consecutive cycles to assess the reproducibility and reversibility of the network recovery.

Cytotoxicity Assessment

The cytotoxicity of the self-healing hydrogels and their chitin nanogel composites was evaluated against L929 murine fibroblast cells using the MTT assay (Xu *et al.* 2012). Cells were cultured in low-glucose DMEM supplemented with 10% FBS and antibiotics at 37 °C in a 5% CO_2 atmosphere. Following ISO 10993-12 (2007), hydrogel extracts were prepared by incubating samples in complete culture medium (0.2 g/mL) at 37 °C for 24 h. L929 cells were seeded in 96-well plates at 1×10^5 cells/well and pre-cultured for 24 h. The medium was then replaced with 75 μL of fresh medium plus 25 μL of extract for treatment groups, or 100 μL of fresh medium for negative controls (n = 6).

After 24, 48, and 72 h of incubation, 10 μL of MTT solution (5 mg/mL) was added to each well. Following 4 h of incubation, the supernatant was aspirated, and the formazan crystals were dissolved in 100 μL of DMSO. Absorbance was measured at 490 nm. Cell viability was calculated as:

Cell Viability (%) = (OD_sample – OD_blank) / (OD_control – OD_blank) × 100%

Cytotoxicity was graded as: Grade 0 (≥ 80%), Grade 1 (60 to 79%), Grade 2 (40 to 59%), Grade 3 (20 to 39%), and Grade 4 (< 20%). The control group contained cells without extract, and the blank contained medium only.

Cellular Adhesion Test

L929 cells at the logarithmic growth phase were seeded into 24-well plates (1 mL/well, 5 × 104 cells/mL). Sterilized material specimens were then immersed in designated wells and incubated at 37 °C for 24 h. After aspirating the culture medium and performing two PBS washes, cells were fixed with 2.5% glutaraldehyde at 4 °C for 24 h. Samples subsequently underwent sequential ethanol gradient dehydration (50%, 70%, 90%, 100%). Blank controls were processed identically without material contact. Following lyophilization and gold sputter-coating, samples were examined using field emission scanning electron microscopy (FE-SEM; ZEISS, Germany). Concurrently, fixed cells were stained with fluorescent dyes, then imaged with a confocal laser scanning microscope (CLSM; Leica TCS SP8, Leica Microsystems GmbH, Germany)

Rabbit Liver Hemostasis Experiment

Male New Zealand rabbits (5 to 6 months, 2.5 to 3.0 kg) were sourced from Vital River Laboratories (Beijing, China). All experimental procedures received prior approval from the Animal Ethics Committee and complied strictly with the National Institutes of Health Guidelines for the Care and Use of Laboratory Animals (NIH Publication No. 85-23, revised 1996). Throughout the acclimatization and study periods, animals were maintained in a comfortable condition: 12-hour light/dark cycles, *ad libitum* access to standard feed and sterilized water, and ambient temperature/humidity regulation.

The hemostatic efficacy of self-healing hydrogels and chitin nanogel-composite self-healing hydrogel was quantitatively evaluated in a standardized rabbit liver incision model (1.5 × 0.5 cm parenchymal defect) using New Zealand White rabbits (n=9) randomized into three cohorts: untreated controls, gauze compression controls; and topical hydrogel injection. Prior to the procedure, anesthesia was induced with intravenous midazolam (0.2–0.5 mg/kg) followed by mask delivery of isoflurane (3–5% for induction, 1–3% for maintenance). Body temperature was maintained using a warming pad and

monitored throughout the anesthetic period. Under general anesthesia, animals were immobilized, abdominally shaved, and disinfected before midline laparotomy exposed the liver. Upon creating the defect and confirming active bleeding, interventions were applied per cohort assignment with simultaneous recording of: (1) time to hemostasis, and (2) blood loss volume *via* gravimetric analysis of pre-positioned subhepatic gauze. Following the completion of the surgical procedure, euthanasia was performed by intravenous administration of pentobarbital sodium (>150 mg/kg) *via* the marginal ear vein until cessation of breathing and cardiac arrest.

Hematoxylin and Eosin (HE) Staining:

Rabbit liver samples were fixed in 4% neutral-buffered formalin, processed through graded alcohols and xylene, then paraffin-embedded and sectioned at 4 μm. Deparaffinized sections were stained with hematoxylin about 10 min, differentiated in acid alcohol, and blued in Scott's tap water, followed by 1 minute eosin counterstaining. Finally, sections were dehydrated, cleared in xylene, mounted with resin, and examined using an OBSERVER D1/AX10 microscope (Zeiss, Germany).

RESULTS AND DISCUSSION

Characterization of Hydrogel Structure

Fourier-transform infrared spectroscopy was systematically employed to monitor the structural evolution and confirm the successful formation of functional groups at each critical stage of the modification and cross-linking process, as comprehensively illustrated in Fig. 1A.

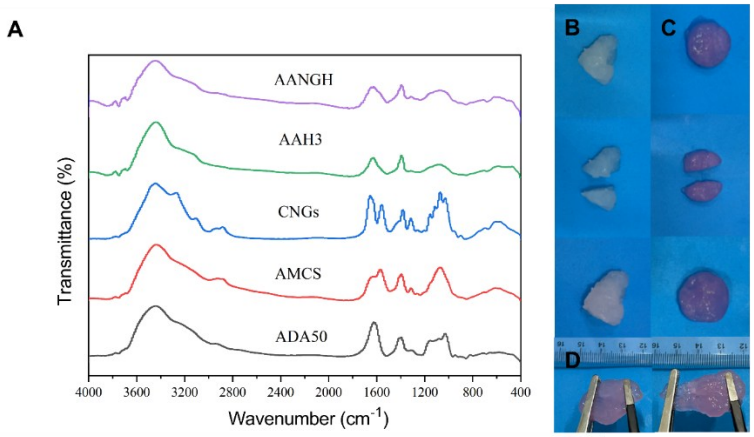

Fig. 1. FT-IR spectra of AANGH and its precursors (A), self-healing process of AAH3 (Pink, B) and AANGH (White, C), and stretchability of AAH3 (D)

The periodate-mediated oxidation of sodium alginate selectively cleaves vicinal diol motifs on the uronate rings to form alginate dialdehyde (ADA50), a transformation clearly evidenced by FT-IR spectroscopy. The spectrum showed a blue shift of the hydroxyl stretch to 3443.3 cm^{-1}, confirming hydroxyl consumption, while preserved carboxylate vibrations at 1622.8 and 1397.3 cm^{-1} indicated maintained backbone integrity and hydrophilicity. The absence of a distinct aldehydic carbonyl band around 1720.0 cm^{-1}

is attributed to intramolecular or intermolecular hemiacetal formation, leading to signal broadening and attenuation (Kang *et al.* 2002; Liu *et al.* 2025).

The spectra of the components provided a baseline, with acrylamide-modified chitosan (AMCS) showing an N-H deformation at 1570.5 cm^{-1} and chitin nanogels (CNGs) displaying distinct N-H stretching at 3269.8 cm^{-1} and NH_2 bending at 1559.6 cm^{-1}, underscoring their amino-rich surfaces. The most critical evidence was found in the final hydrogels. The appearance of new bands at 1626.8 cm^{-1} (AAH3) and 1625.6 cm^{-1} (AANGH) is unequivocally attributed to the imine bond (C=N) stretching of a Schiff base, providing direct spectroscopic proof of the dynamic covalent network formed between AMCS amino groups and ADA50 aldehydes that underpins the material's self-healing and injectable properties. The slight wavenumber difference suggests a potential subtle interaction between the CNGs and the polymer matrix, further reinforcing the successful integration of the nanofiller.

Self-healing Property of Hydrogels

The self-healing hydrogels were successfully synthesized *via* dynamic Schiff base linkages (-CH=N-) formed between the primary amino groups on acrylamide-modified chitosan (AMCS) and the aldehyde functionalities on oxidized alginate (ADA50), with the reversibility of these imine bonds being the cornerstone of the material's autonomous repair capability. This inherent reversibility enables the network to undergo continuous dissociation and reformation in response to damage, facilitating molecular reconnection across fractured interfaces.

A compelling macroscopic demonstration is shown in Fig. 1B, where a bisected specimen of the AAH3 hydrogel spontaneously healed at room temperature after the cut surfaces were brought into gentle contact. A similarly prominent and efficient self-healing capability was also evidenced in the chitin nanogel-composite hydrogel (AANGH), confirming that the incorporation of CNGs does not hinder the dynamic cross-linking process (Fig. 1C).

Notably, systematic investigation revealed that the self-healing efficiency is profoundly influenced by the stoichiometric balance of the precursors, specifically the ADA50 content. While a higher ADA50 proportion increases initial cross-linking density, it reduces the population of free amino groups essential for reversible bond reformation at the damage interface, thereby impairing dynamic reconfigurability and extending recovery time. As summarized in Fig. 1D, the AAH1 formulation—with lower ADA50 content and abundant free amino groups—displayed outstanding self-healing but compromised mechanical integrity, whereas AAH3 achieved an optimal balance of autonomous repair, mechanical strength, and stretchability for practical application.

Rheological Properties of Self-healing Hydrogels

Rheological characterization was pivotal in quantifying the viscoelastic properties and dynamic performance of the synthesized hydrogels. Oscillatory strain sweep measurements performed within the linear viscoelastic region (LVR) confirmed a dominant solid-like, gel-state behavior for both the AAH3 and AANGH hydrogels. This was conclusively evidenced by the storage modulus (G'), representing the elastic energy stored in the material, substantially surpassing the loss modulus (G''), which corresponds to the viscous dissipation, as graphically presented in Fig. 2A. This $G' > G''$ relationship is

a fundamental indicator of a stable, cross-linked elastic network formation, which forms the mechanical foundation for these self-healing systems.

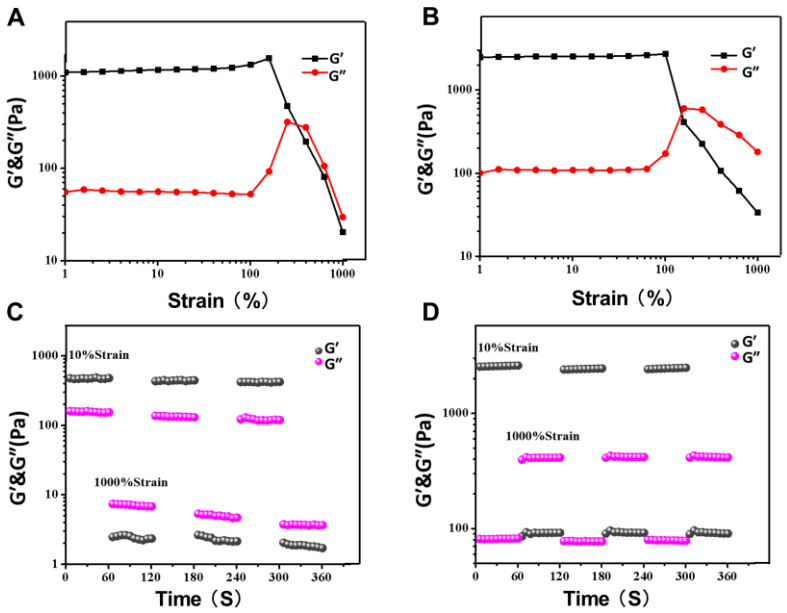

Fig. 2. Strain sweep of AAH3 (A) and AANGH (B) and alternate strain sweep of AAH3 (C) and AANGH (D)

The dynamic nature of the Schiff base cross-links was revealed under increasing deformation, where a sharp drop in G' occurred beyond 100% strain, culminating in a characteristic G'–G'' crossover around 150% strain that reflects a reversible transition from a solid-like gel to a fluid-like sol state. This can be mechanistically attributed to the rate-limiting dissociation of imine bonds under high shear. A key finding is that the incorporation of chitin nanogels (CNGs) into the AANGH composite notably enhanced the overall viscoelastic performance, simultaneously elevating both G' and G'' values. This finding indicates that CNGs act as multifunctional reinforcing fillers without compromising the network's dynamic character (Fig. 2A).

The exceptional reversibility of these networks was further probed through cyclic step-strain recovery tests. As shown in Fig. 2B, the AAH3 hydrogel exhibited a rapid decrease in G' under high strain (1000%), suggesting temporary network disassembly, but critically, it recovered instantaneously and completely upon returning to low strain (10%), providing direct rheological proof of the superb dynamic reversibility and self-healing capability of the cross-linked network. Notably, under identical conditions, the AANGH composite demonstrated consistently higher G' and G'' values in each cycle, translating to superior network strength, improved resistance to deformation-driven breakdown, and an overall reinforcement of the material's self-healing capability for injectable applications.

Cytocompatibility of Chitin Nanogel-composite Self-healing Hydrogels

The exceptional self-healing performance of the AANGH composite hydrogel was paralleled by outstanding biocompatibility, as evidenced by comprehensive in vitro assessments. Quantitative MTT assay data revealed that the viability of L929 fibroblast cells cultured in extracts of both AAH3 and AANGH consistently remained at or above

100% across 24, 48, and 72-hour incubation periods, indicating negligible cytotoxicity and suggesting that the hydrogel degradation products may even support a favorable metabolic environment for cell growth (Fig. 3A).

Beyond cell survival, qualitative morphological analysis *via* FE-SEM and CLSM provided critical insights, revealing a distinct advantage of the AANGH composite. A considerably higher proportion of L929 cells cultured in the presence of AANGH exhibited the characteristic spindle-shaped, well-spread morphology of healthy, proliferating fibroblasts, along with increased cell density and more extensive cytoskeletal development (Fig. 3B). These clear indicators of excellent cell health and adhesion directly corroborate the quantitative MTT findings, confirming the material's viability for practical biomedical use.

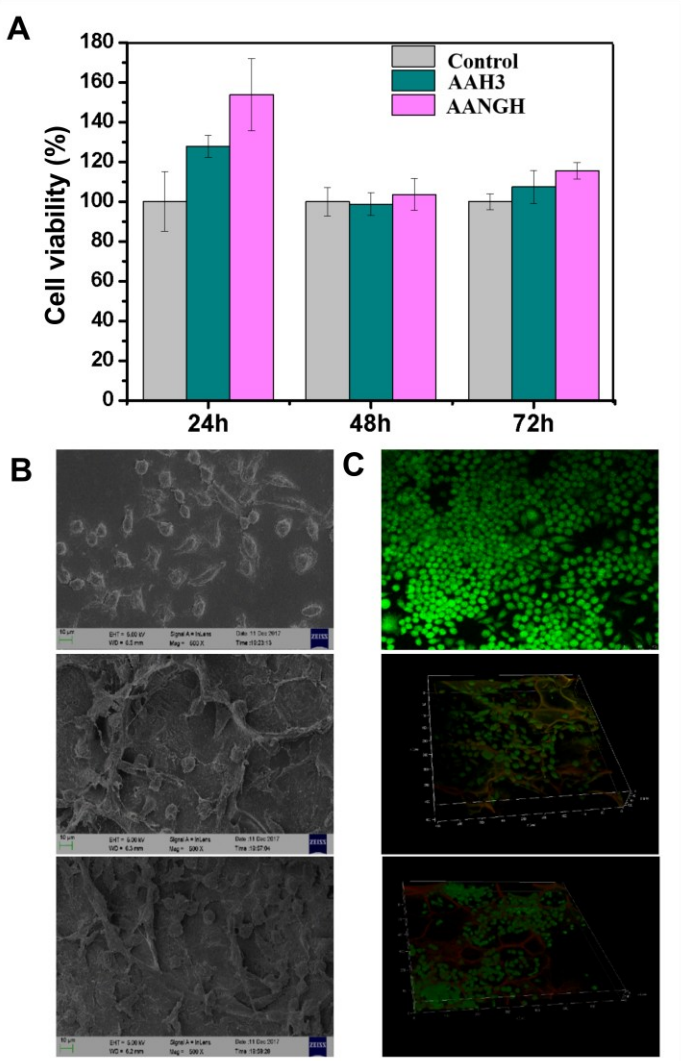

Fig. 3. Cell viability of L929 cells cultured with AAH3and AANGH after 24 h, 48 h, and 72 h (A), and the morphology (B,Scale bar: 10μm) and viability (C) of L929 cells in the control, AAH3, and AANGH (top to bottom) groups characterized by FE-SEM and CLSM, respectively. Data represent the mean ± SD (n = 6); *p < 0.05, **p < 0.01.

Collectively, this multi-faceted biological evaluation provides a compelling case for the biosafety of the developed hydrogels. The results conclusively confirmed the non-toxic nature of both the AAH3 and AANGH formulations. More importantly, they demonstrated that the incorporation of chitin nanogels (CNGs) in AANGH did not induce adverse cellular effects; in contrast, it conferred superior biocompatibility compared to the AAH3 matrix. This enhanced cellular affinity is likely attributable to the nanofibrous structure of the CNGs, which may better mimic the native extracellular matrix, thereby providing a more conducive microenvironment for cell attachment and proliferation. This crucial evidence, integrating both quantitative data and qualitative imaging from Fig. 3, strongly supports the potential biosafety of the AANGH hydrogel for future practical applications.

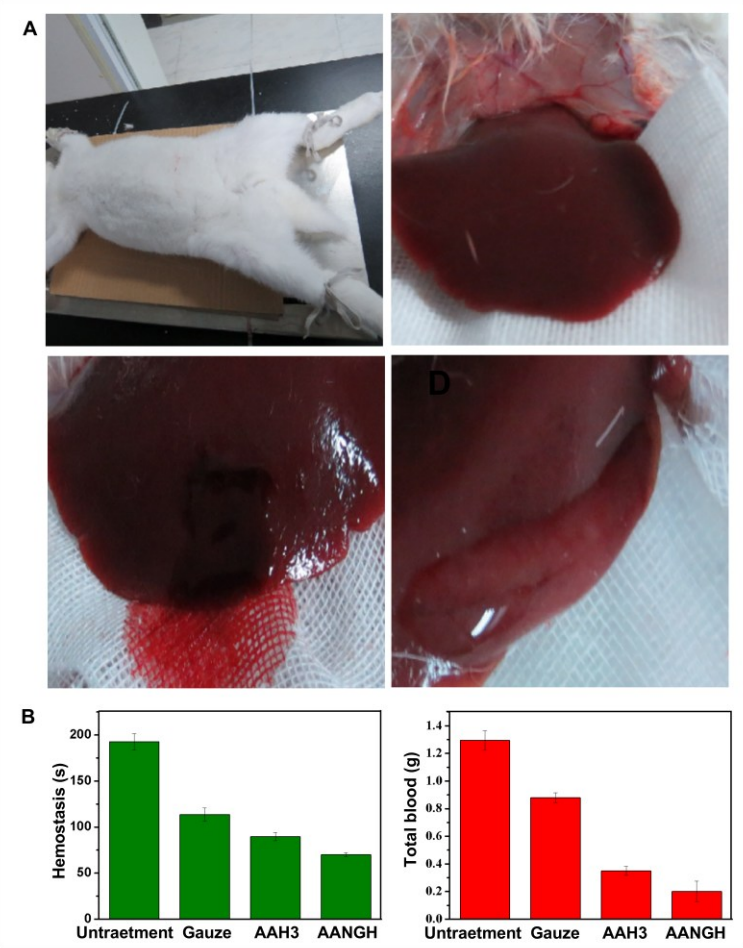

Fig. 4. Surgical procedure of rabbit liver hemostasis experiment(A): rabbit anesthetization and fixation; Laparotomy for liver exposure; 1 × 0.3 cm transverse incision creation of liver; self-healing hydrogels injection achieving hemostasis. Total blood loss and hemostasis time(B) for control group (no treatment), gauze group (covered with 50g weight), AAH3 and AANGH group (adhesive injection). Data represents the mean ± SD (n = 6). *p < 0.05, **p < 0.01.

Rabbit Liver Hemostatic Efficacy of Chitin Nanogel-Composite Self-Healing Hydrogels

Crosslinking ADA50 and AMCS brought about the synthesis of AAH3, whose enhanced mechanical properties and self-healing capability stem from dynamic Schiff base bonds formed between their amino and aldehyde groups, respectively. In rabbit liver injury

models, AAH3 injection achieved effective hemostasis while significantly reducing bleeding time, total blood loss, and iatrogenic trauma risks compared to conventional gauze compression (Fig. 4A). Further comparative analysis demonstrated that AANGH possesses superior hemostatic efficacy to AAH3, with its injection resulting in significantly lower blood loss and accelerated wound healing compared to AAH3 (Fig. 4B). Consequently, AANGH demonstrates enhanced hemostatic efficacy compared to AAH3 for controlling hemorrhage in adhesive wound contexts.

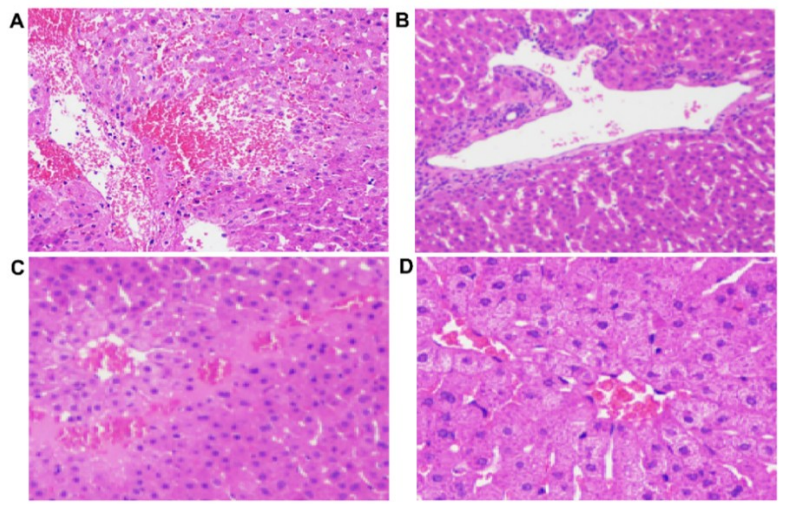

Fig. 5. HE staining of wound tissues of control group (no treatment) (A), gauze group (covered with 50g weight) (B), AAH3 and AANGH group (adhesive injection) (C and D). Scale bar = 50 μm

Antibacterial Activity of Chitin Nanogel-Composite Self-Healing Hydrogels

In the antibacterial study of AAH3 and AANGH, H&E staining analysis of perihepatic tissue samples revealed that the number of inflammatory cells (blue regions) correlated with the severity of tissue inflammation and infection (Fig. 5). Compared to controls, both AAH3 and AANGH reduced inflammatory cell infiltration, with AANGH showing the lowest counts. This confirms AANGH's superior efficacy in attenuating hepatic inflammation and infection.

CONCLUSIONS

1. Structural analysis *via* Fourier transform infrared (FT-IR) spectroscopy provided definitive evidence for the underlying chemical mechanism. The characteristic imine (C=N) stretching bands observed in the hydrogels (AAH3 and AANGH) confirmed the successful formation of dynamic Schiff base linkages between the amino groups of AMCS and the aldehyde groups of ADA50. This reversible covalent bonding is the fundamental principle enabling the material's autonomous self-healing and injectable characteristics.
2. The macroscopic self-healing experiments and rheological assessments revealed a critical balance between mechanical integrity and reparability. While the AAH3 formulation was identified as an optimal compromise, the incorporation of chitosan nanogels (CNGs) into the AANGH composite marked a notable advancement. Rheological data unequivocally demonstrated that AANGH possessed superior

viscoelastic properties, including a higher storage modulus (G') and enhanced recovery under cyclic strain. This indicates a more robust and resilient network, offering greater resistance to deformation without sacrificing the dynamic reversibility that facilitates excellent self-healing.

3. The critical aspect of biocompatibility was rigorously addressed through *in vitro* cytocompatibility assays. The 3-(4,5-dimethylthiazol-2-yl)-2,5-diphenyltetrazolium bromide (MTT) results, showing cell viability at or above 100%, coupled with supportive morphological data from field emission scanning electron microscopy (FE-SEM) and confocal laser scanning microscopy (CLSM), confirmed that both AAH3 and AANGH exhibited negligible cytotoxicity. Notably, the AANGH composite fostered a denser and more healthy fibroblast morphology, suggesting its nanogel-reinforced structure provides a more favorable microenvironment for cells, thereby establishing a strong foundation for its biosafety. It synergistically combines the injectability and self-healing afforded by dynamic covalent chemistry with the greatly enhanced mechanical strength and cytocompatibility imparted by the CNG filler.
4. In a rabbit liver trauma model, *in vivo* experiments further confirmed the excellent hemostatic and anti-inflammatory functions of this hydrogel system. Compared to the untreated group and the traditional gauze compression group, injection of the AAH3 hydrogel significantly shortened the hemostasis time and reduced total blood loss. More importantly, the nanocomposite hydrogel AANGH demonstrated even more superior performance, with faster hemostasis and less blood loss, indicating that the introduction of CNGs significantly enhanced the material's immediate hemostatic capability. Histological analysis revealed that the AANGH-treated group had the lowest degree of inflammatory cell infiltration in the peri-wound tissue, confirming that while achieving effective hemostasis, it also better controlled local inflammation and infection, highlighting its comprehensive advantages as a multifunctional hemostatic dressing.

The AANGH hydrogel developed in this study enhanced mechanical properties, sped up hemostasis, and provided anti-inflammatory effects. The hemostatic effect was likely achieved through a synergistic interplay: the high water-absorbing capacity of oxidized sodium alginate concentrates blood components, working in concert with the calcium ion-binding ability and antibacterial properties of carboxymethyl chitosan. Furthermore, the authors have speculated the potential mechanisms by which CNGs enhance hemostasis, primarily through enhancing tissue adhesive capability and stable physical barrier formation. However, its molecular mechanisms of hemostasis remain to be elucidated, and its long-term biosafety, multifunctional integration, and applicability in extreme hemorrhagic conditions require systematic validation. Therefore, future research should focus on elucidating its mechanisms of action and expanding its intelligent functionalities and clinical translation potential.

ACKNOWLEDGMENTS

This study was supported by the Postdoctoral Fellowship Program of CPSF under Grant Number GZC20232426, the Key Scientific and Technological Research Projects in Henan Province (242102230174), Joint Fund Project of Natural Science Foundation of

Hunan Province (2025JJ80244), and the Technological Innovation Fund of Hunan Forestry Department (XLKY202202).

REFERENCES CITED

Bi, S., Pang, J., Huang, L., Sun, M., Cheng, X., and Chen, X. (2020). "The toughness chitosan-PVA double network hydrogel based on alkali solution system and hydrogen bonding for tissue engineering applications," *Int. J. Biol. Macromol.* 146, 99-109. https://doi.org/10.1016/j.ijbiomac.2019.12.186

Cao, J., You, J., Zhang, L., and Zhou, J. (2018). "Homogeneous synthesis and characterization of chitosan ethers prepared in aqueous alkali/urea solutions," *Carbohydr. Polym.* 185, 138-144. https://doi.org/10.1016/j.carbpol.2018.01.010

Faizuloev, E., Marova, A., Nikonova, A., Volkova, I., Gorshkova, M., and Izumrudov, V. (2012). "Water-soluble N-[(2-hydroxy-3-trimethylammonium)propyl]chitosan chloride as a nucleic acids vector for cell transfection," *Carbohydr. Polym.* 89(4), 1088-1094. https://doi.org/10.1016/j.carbpol.2012.03.071

Fan, P., Zeng, Y., Zaldivar-Silva, D., Agüero, L., and Wang, S. (2023). "Chitosan-based hemostatic hydrogels: The concept, mechanism, application, and prospects," *Molecules* 28(3), article 1473. https://doi.org/10.3390/molecules28031473

Goncharuk, O., Korotych, O., Samchenko, Y., Kernosenko, L., Kravchenko, A., Shtanova, L., Tsymbalyuk, O., Poltoratska, T., Pasmurtseva, N., Mamyshev, I., *et al.* (2021). "Hemostatic dressings based on poly(vinyl formal) sponges," *Materials Science and Engineering: C* 129, article 112363. https://doi.org/10.1016/j.msec.2021.112363

Guo, B.L., and Gao, Q.Y. (2007). "Preparation and properties of a pH/temperature-responsive carboxymethyl chitosan/poly(N-isopropylacrylamide)semi-IPN hydrogel for oral delivery of drugs," *Carbohydr. Res.* 342(16), 2416-2422. https://doi.org/10.1016/j.carres.2007.07.007

Huang, W., Cheng, S., Wang, X., Zhang, Y., Chen, L., and Zhang, L. (2021). "Noncompressible hemostasis and bone regeneration induced by an absorbable bioadhesive self-healing hydrogel," *Adv. Funct. Mater.* 31(22), article 2009189. https://doi.org/10.1002/adfm.202009189

Kang, H.-A., Shin, M. S., and Yang, J.-W. (2002). "Preparation and characterization of hydrophobically modified alginate," *Polym. Bull.* 47(5), 429-435. https://doi.org/10.1007/s002890200005

Li, C., Zhang, X., Zhou, C., Yang, F., Liang, J., Gu, H., Wang, J., Wang, F., Peng, W., Guo, J.,and Li, H. (2024). "Performance and mechanism of a novel bamboo-based magnetic biochar composite for efficient removal of norfloxacin," *Adv. Compos. Hybrid Mater.* 8(1), article 71. https://doi.org/10.1007/s42114-024-01142-8

Liu, X., Hu, J., Hu, Y., Liu, Y., Wei, Y., and Huang, D. (2025). "Multifunctional injectable oxidized sodium alginate/carboxymethyl chitosan hydrogel for rapid hemostasis," *Colloids and Surfaces B: Biointerfaces* 245, article 114346. https://doi.org/10.1016/j.colsurfb.2024.114346

Liu, Y., Zhang, X. L., Du, Y. Z., Du, X. B. Zhang, Y., Deng, L.Y., Li, C., and Guo, J. H. (2025). "Functionalization of wood for the removal of heavy metal ions from waster water: A review," *Forests* 16, article 1684. https://doi.org/10.3390/f16111684

Ma, S., Chen, K., Ding, Q., Zhang, S., lu, Y., Yu, T., Ding, C., Liu, W., and liu, S. (2024). "Quaternized oxidized sodium alginate injectable hydrogel with high antimicrobial and hemostatic efficacy promotes diabetic wound healing," *International Journal of Pharmaceutics* 661, article 124421. https://doi.org/10.1016/j.ijpharm.2024.124421

Pourshahrestani, S., Zeimaran, E., Kadri, N. A., Mutlu, N., and Boccaccini, A. R. (2020). "Polymeric hydrogel systems as emerging biomaterial platforms to enable hemostasis and wound healing," *Adv. Healthcare Mater.* 9(20), article 2000905. https://doi.org/10.1002/adhm.202000905

Qiao, Z., Lv, X., He, S., Bai, S., Liu, X., Hou, L., He, J., Tong, D., Ruan, R., Zhang, J., *et al.* (2021). "A mussel-inspired supramolecular hydrogel with robust tissue anchor for rapid hemostasis of arterial and visceral bleedings," *Bioact. Mater.* 6(9), 2829-2840. https://doi.org/10.1016/j.bioactmat.2021.01.039

Ravichandran, V., and Jayakrishnan, A. (2018). "Synthesis and evaluation of anti-fungal activities of sodium alginate-amphotericin b conjugates," *International Journal of Biological Macromolecules* 67(11), 4317-4322. https://doi.org/ 10.1016/j.ijbiomac.2017.11.030

Tompeck, A. J., Gajdhar, A. R., Dowling, M., Johnson, S. B., Barie, P. S., Winchell, R. J., King, D., Scalea, T. M., Britt, L. D., and Narayan, M. (2020). "A comprehensive review of topical hemostatic agents: The good, the bad, and the novel," *J. Trauma Acute Care Surg.* 88(1), article 2508. https://doi.org/10.1097/TA.0000000000002508

Vo, D.-T., Sabrina, S., and Lee, C.-K. (2017). "Silver deposited carboxymethyl chitosan-grafted magnetic nanoparticles as dual action deliverable antimicrobial materials," *Materials Science and Engineering: C* 73, 544-551. https://doi.org/10.1016/j.msec.2016.12.066

Xu, X., Gu, Z., Chen, X., Shi, C., Liu, C., Liu, M., Wang, L., Sun, M., Zhang, K., Liu, Q., *et al.* (2019). "An injectable and thermosensitive hydrogel: Promoting periodontal regeneration by controlled-release of aspirin and erythropoietin," *Acta Biomater.* 86, 235-246. https://doi.org/10.1016/j.actbio.2019.01.001

Xu, Y., Li, L., Yu, X., Gu, Z., and Zhang, X. (2012). "Feasibility study of a novel crosslinking reagent (alginate dialdehyde) for biological tissue fixation," *Carbohydr. Polym.* 87(2), 1589-1595. https://doi.org/10.1016/j.carbpol.2011.09.059

Yang, J., Wang, T., Zhang, L., Fan, P., Zhao, J., Zheng, X., Lai, Y., Liu, H., and Wang, S. (2024). "Injectable hemostatic hydrogel adhesive with antioxidant, antibacterial and procoagulant properties for hemorrhage wound management," *J. Colloid Interface Sci.* 673, 395-410. https://doi.org/10.1016/j.jcis.2024.05.207

Yang, Z., Chen, L., Liu, J., Zhuang, H., Lin, W., Li, C., and Zhao, X. (2023). "Short peptide nanofiber biomaterials ameliorate local hemostatic capacity of surgical materials and intraoperative hemostatic applications in clinics," *Adv. Mater.* 35(39), article 2301849. https://doi.org/10.1002/adma.202301849

Ye, R., Zhu, Z., Gu, T., Cao, D., Jiang, K., Dai, Q., Xing, K., Jiang, Y., Zhou, S., Cai, P., *et al.* (2024). "Neutrophil extracellular traps-inspired DNA hydrogel for wound hemostatic adjuvant," *Nat. Commun.* 15(1), article 5557. https://doi.org/10.1038/s41467-024-49933-3

Zhang, B. , Wang, M. , Tian, H. , Cai, H. , Wu, S. , and Jiao, S. , *et al.* (2024). "Functional hemostatic hydrogels: Design based on procoagulant principles," *Journal of Materials Chemistry, B: Materials for Biology and Medicine* 12(7), article 24. https://doi.org/10.1039/D3TB01900D

Zhang, C., Tan, C., Shen, H., Xu, Q., Pan, J., and Wang, X. (2024). "Synthesis, characterization, and application potential of chitosan/acrylamide composite hydrogels as skin expanders," *J. Mater. Sci.:Mater. Med.* 35(1), article 72. https://doi.org/10.1007/s10856-024-06812-z

Zhang, L., Wang, L., Guo, B., and Ma, P. X. (2014). "Cytocompatible injectable carboxymethyl chitosan/N-isopropylacrylamide hydrogels for localized drug delivery," *Carbohydr. Polym.* 103, 110-118. https://doi.org/10.1016/j.carbpol.2013.12.017

Zhang, S. , Lei, X. , Lv, Y. , Wang, L., and Wang, L. N. (2024). "Recent advances of chitosan as a hemostatic material: Hemostatic mechanism, material design and prospective application," *Carbohydrate Polymers: Scientific and Technological Aspects of Industrially Important Polysaccharides* 327, article 121673. https://doi.org/10.1016/j.carbpol.2023.121673

Zhao, L., Feng, Z., Lyu, Y., Yang, J., Lin, L., Bai, H., Li, Y., Feng, Y., and Chen, Y. (2023). "Electroactive injectable hydrogel based on oxidized sodium alginate and carboxymethyl chitosan for wound healing," *Int. J. Biol. Macromol.* 230, article 123231. https://doi.org/10.1016/j.ijbiomac.2023.123231

Zhao, X., Wu, H., Guo, B., Dong, R., Qiu, Y., and Ma, P. X. (2017). "Antibacterial anti-oxidant electroactive injectable hydrogel as self-healing wound dressing with hemostasis and adhesiveness for cutaneous wound healing," *Biomaterials* 122, 34-47. https://doi.org/10.1016/j.biomaterials.2017.01.011

Ziaei, A. A. , Erfan-Niya, H. , Fathi, M. , and Amiryaghoubi, N. (2023). "In situ forming alginate/gelatin hybrid hydrogels containing doxorubicin loaded chitosan/aunps nanogels for the local therapy of breast cancer," *International Journal of Biological Macromolecules* 246, article 125640. https://doi.org/10.1016/j.ijbiomac.2023.125640

Article submitted: November 19, 2025; Peer review completed: December 13, 2025; Revised version received: January 3, 2026; Accepted: January 4, 2026; Published: January 30, 2026.
DOI: 10.15376/biores.21.1.2438-2453